Mechanism of fast lattice diffusion of hydrogen in palladium: Interplay of quantum fluctuations and lattice strain

Hajime Kimizuka,[1,*] Shigenobu Ogata,[1,2] and Motoyuki Shiga[3]
[1]*Department of Mechanical Science and Bioengineering, Osaka University, Osaka 560-8531, Japan*
[2]*Center for Elements Strategy Initiative for Structural Materials, Kyoto University, Kyoto 606-8501, Japan*
[3]*Center for Computational Science and E-Systems, Japan Atomic Energy Agency, Chiba 277-0871, Japan*

(Received 1 August 2017; revised manuscript received 24 November 2017; published 10 January 2018)

Understanding the underlying mechanism of the nanostructure-mediated high diffusivity of H in Pd is of recent scientific interest and also crucial for industrial applications. Here, we present a decisive scenario explaining the emergence of the fast lattice-diffusion mode of interstitial H in face-centered cubic Pd, based on the quantum mechanical natures of both electrons and nuclei under finite strains. *Ab initio* path-integral molecular dynamics was applied to predict the temperature- and strain-dependent free energy profiles for H migration in Pd over a temperature range of 150–600 K and under hydrostatic tensile strains of 0.0%–2.4%; such strain conditions are likely to occur in real systems, especially around the elastic fields induced by nanostructured defects. The simulated results revealed that, for preferential H location at octahedral sites, as in unstrained Pd, the activation barrier for H migration (Q) was drastically increased with decreasing temperature owing to nuclear quantum effects. In contrast, as tetrahedral sites increased in stability with lattice expansion, nuclear quantum effects became less prominent and ceased impeding H migration. This implies that the nature of the diffusion mechanism gradually changes from quantum- to classical-like as the strain is increased. For H atoms in Pd at the hydrostatic strain of $\sim$2.4%, we determined that the mechanism promoted fast lattice diffusion ($Q = 0.11$ eV) of approximately 20 times the rate of conventional H diffusion ($Q = 0.23$ eV) in unstrained Pd at a room temperature of 300 K.

DOI: 10.1103/PhysRevB.97.014102

I. INTRODUCTION

The Pd-H system has received much attention, not only from fundamental interest in the physics and chemistry of a prototype metal-H system [1–3], but also because of several technological applications using H_2 gas as an energy carrier and source of fuel. This is because Pd is a promising candidate for H-absorbing and H-permeable materials for the reason that it can absorb, transport, and release large amounts of H at moderate temperature and pressure conditions [3]. In particular, nonporous membranes of Pd and Pd alloys have been extensively studied for utilization in H-purification devices or fuel cells because they are highly selective for H separation (see Refs. [4,5]). The effectiveness of the membranes for H permeation relies on the dissociation of molecular H_2 at the membrane surface, the solubility of atomic H in interstitial sites of the metal, and rapid diffusive transport of atomic H through interstitial sites. Elucidating the rate of diffusion of H in Pd is important for understanding the kinetics of H storage and permeation; however, a consensus on the physical mechanism of H diffusivity in the metal is still lacking.

Much attention has focused on clarifying the mechanism of the high diffusivity of H in nanostructured Pd, such as nanocrystalline grain boundaries [6–8], nanoparticles [9,10], and dislocation cores [11,12]. Kofu *et al.* [9] recently examined the diffusion dynamics of H in 8-nm Pd nanoparticles using quasielastic neutron scattering and observed a fast relaxation process with the small activation energy of 0.12 eV, in addition to a conventional relaxation process (0.24 eV) inside the $PdH_{0.47}$ nanoparticles. The face-centered cubic (fcc) lattice (space group: $Fm\bar{3}m$) of Pd has two possible interstitial sites for H atoms, i.e., octahedral (O) sites (4*b* positions in Wyckoff notation) and tetrahedral (T) sites (8*c* positions). Although H and deuterium (D) atoms in bulk Pd prefer O sites to T sites, a recent neutron powder diffraction experiment [10] suggested that a relatively large fraction of D atoms were located at T sites in the $PdD_{0.363}$ nanoparticles. Because an increase in the lattice constant (by up to 1.9%) was locally observed in the pristine Pd nanoparticle samples [9,10], the lattice expansion/distortion was supposed to affect the ground states and dynamics of H (and D) in some manner. However, the results obtained, so far, do not provide evidence for a consistent interpretation of the primary mechanism for the phenomena involved. In particular, it must be considered that the site occupancy can differ for different isotopes such as D and tritium because of the quantum nature of light nuclei.

Large lattice expansions on the order of a few percent are often observed in local regions of heterogeneous structures, especially in nanomaterials. This originates from (i) the lattice mismatch in heterophase boundaries [13,14] (e.g., core-shell structures and heteroepitaxial interfaces), (ii) the elastic strain fields generated around defects [11,12] (e.g., dislocations, precipitates, and microcracks), (iii) impurity doping and alloying with large-size elements [5], and (iv) the formation of hydrides/oxides [14–16]. The introduction of such lattice imperfections to crystalline metal produces a lattice expansion that typically generates a multiaxial tensile (expansive) strain

*Corresponding author: kimizuka@me.es.osaka-u.ac.jp

field. The behavior of H in a nanoscale heterogeneous structure is considered to be dominated by the complex coupling between chemo-physical and mechanical effects, depending on the magnitude and type of intrinsic strain.

First-principles calculations have been used to study H dissolution, diffusion, and trapping energetics in the case of fcc Pd in many studies [12,17–21]. Modern electronic-structure calculations based on density functional theory (DFT) can provide good descriptions of the geometries, energetics, and potential energy surfaces in Pd-H systems. However, to the best of the authors' knowledge, no conclusive explanation exists for the manner in which the direct coupling of nuclear quantum effects and lattice-strain effects is exhibited. In principle, a quantum mechanical description of both electrons and nuclei is necessary to understand the site preference and diffusivity of H, while considering the relaxation of the surrounding lattice as well. In this context, an atomistic approach based on Feynman's path-integral (PI) theory [22] could be quite effective in the precise description of metal-H systems involving the effects of quantum fluctuations and zero-point motion of H (see, for example, Refs. [21,23–32]). Such *ab initio* modeling can serve as a realistic and practical solution for understanding the possible mechanisms of H diffusion in Pd under strained conditions.

In this study, we investigated the issues related to the emergence of a fast diffusion process of H in elastically strained fcc Pd. Our calculations were based on *ab initio* path-integral molecular dynamics (PIMD) in the DFT framework. The PIMD calculations, combined with an *ab initio* evaluation of interactions using electronic structure theory, incorporated the quantum mechanical natures of both the electrons and nuclei. We characterized the quantum effects on the activation barriers and site energies for H migration between the O and the T interstitial sites, according to the PIMD-based free energy profiles calculated over a wide temperature range. Using the obtained energetics, we determined that the fcc Pd lattice permits a mechanism for the fast diffusion of H, which is induced by the explicit coupling of the effects of quantum fluctuations and lattice expansion.

II. METHODS

A. DFT calculations

The electronic-structure calculations were performed within DFT using the Vienna *ab initio* simulation package (VASP) [33], which employs a plane-wave basis to represent the wave functions of the valence electrons. The interactions of ionic cores and valence electrons were described using the projector-augmented wave (PAW) method [34,35]. The valence electron configurations considered in this study included $4d^{10}$ for Pd and $1s^1$ for H. The exchange-correlation functional was described within the generalized gradient approximation (GGA) of Perdew, Burke, and Ernzerhof (PBE) [36]. To check the sensitivity of the exchange-correlation functionals to the energetics of the Pd-H system, the local-density approximation (LDA) functional [37,38] was also applied and the results were compared to those obtained from the GGA functional in selected cases (see Appendix A).

Because H atoms jump between neighboring interstitial sites in bulk Pd, the minimum-energy path (MEP) and the transition state for H migration between the closest O and T sites were obtained using the nudged elastic band (NEB) method [39] based on DFT. We considered the $Pd_{32}H$ supercell with dimensions of $2a \times 2a \times 2a$ (where a is the lattice constant of the fcc unit cell) under periodic boundary conditions, in which one H atom was initially placed at one of the O or T sites in the fcc structure. The cell parameters and atomic positions were relaxed within the classical DFT regime (i.e., without nuclear quantum effects) until the residual forces acting on each atom were less than 10 meV/Å using the Methfessel-Paxton smearing method [40] with a width of 0.2 eV. An interpolated chain of configurations (images) between the initial and final geometries, in which the H atom was located at the O and T sites, respectively, was connected by springs and simultaneously relaxed to obtain the MEP. The number of images between the initial and final states in the MEP was set as 11. During the NEB calculations, the cell volume was maintained at the average of those of the initial- and final-state geometries of the H-migration process as the ionic coordinates were relaxed. All the calculations were performed with a plane-wave energy cutoff of 300–400 eV using a $6 \times 6 \times 6$ or $16 \times 16 \times 16$ Monkhorst-Pack $\boldsymbol{k}$-point mesh [41] for integration over the Brillouin zone.

B. PIMD calculations

To investigate the effects of quantum fluctuations on the site preference and migration barrier of H in Pd, the PIMD method [42,43] was employed. The PIMD approach provides an effective and versatile route to compute the static properties of quantum systems at finite temperatures (without *real-time* dynamical information), in which the partition function of a quantum particle can be expressed as a configurational integral of a classical object. This object can be approximated as a closed ring polymer (or necklace) consisting of discrete monomers (or beads) connected via harmonic springs with equilibrium distances all equal to zero. The spring constant of the ring polymers is $m_I P/(\beta\hbar)^2$, where m_I represents the mass of the Ith quantum particle in the N-particle system ($1 \leqslant I \leqslant N$); P, the number of beads in each ring polymer; β, the inverse temperature $(kT)^{-1}$; k, the Boltzmann constant; T, the absolute temperature; and $\hbar$, the Planck constant. While exact results are obtained in the limit $P \to \infty$, a large but finite number of beads can be chosen for a given system and temperature such that the induced systematic error is within the numerical accuracy of the simulation.

In the *ab initio* PIMD [44,45], a statistical ensemble of bead configurations $\{\boldsymbol{r}_I^{(s)}\}$ ($1 \leqslant I \leqslant N$, $1 \leqslant s \leqslant P$) is generated according to the discrete PI expression for the partition function of N quantum nuclei, which is given by

$$Z(\beta) = \lim_{P\to\infty}\left[\prod_{I=1}^{N}\left(\frac{m_I P}{2\pi\beta\hbar^2}\right)^{\frac{3P}{2}}\int d\boldsymbol{r}_I^{(1)}\cdots\int d\boldsymbol{r}_I^{(P)}\right] \times \exp\left(-\beta V_{\mathrm{eff}}\left[\left\{\boldsymbol{r}_I^{(s)}\right\}\right]\right). \quad (1)$$

Here, $V_{\rm eff}[\{\boldsymbol{r}_I^{(s)}\}]$ denotes the effective potential defined as

$$V_{\rm eff}[\{\boldsymbol{r}_I^{(s)}\}] \equiv \sum_{s=1}^{P}\left[\sum_{I=1}^{N}\frac{m_I P}{2\beta^2\hbar^2}\left(\boldsymbol{r}_I^{(s+1)}-\boldsymbol{r}_I^{(s)}\right)^2 + \frac{1}{P}V\left(\boldsymbol{r}_1^{(s)},\cdots,\boldsymbol{r}_N^{(s)}\right)\right] \quad (2)$$

with the cyclic boundary condition, $\boldsymbol{r}_I^{(P+1)} = \boldsymbol{r}_I^{(1)}$. We should note that the interaction potential $V(\boldsymbol{r}_1^{(s)},\ldots,\boldsymbol{r}_N^{(s)})$, which acts between beads with the same bead index s, is obtained by calculating the ground-state energy of the electrons based on DFT (within the adiabatic approximation) for N nuclei fixed in the positions of the sth bead configuration. The ensemble average of a quantity according to Eq. (1) is denoted by angle brackets $\langle\rangle_{\rm PI}$ hereafter.

To uncouple the harmonic bead-bead interaction term, the bead coordinates were transformed to normal-mode coordinates [42,46]. The fictitious masses associated with the normal-mode momenta were chosen to achieve efficient sampling by setting all chain frequencies to the same value, i.e., $\tilde{m}_I^{(1)} = m_I$, $\tilde{m}_I^{(j)} = \lambda_j m_I$ $(2 \leqslant j \leqslant P)$, where $\{\lambda_j\}$ are a set of normal-mode frequencies. In addition, a massive thermostatting scheme was used in PIMD by attaching separate Nosé-Hoover chains [47] with lengths of three to all degrees of freedom, in order to assure ergodic sampling of the phase space. For each temperature condition (150–600 K), PIMD calculations were performed in the canonical ensemble for 1000 steps with the time increment $\Delta t = 1$ fs. In these calculations, the multiple-time-step method based on the reference system propagator algorithm [48] was employed for time integration; the harmonic forces and physical forces were updated at intervals of $\frac{1}{50}\Delta t$ and Δt, respectively.

C. Free energy profile

To characterize the change in the apparent activation barrier with temperature, we evaluated the differences between the free energies of the system for H located at interstitial O, T, and saddle-point (S) sites using the PIMD method; the classical system of ring polymers isomorphic to a set of quantum nuclei was simulated by a molecular dynamics method; and then the static averages (e.g., mean forces and spatial distributions) were calculated by sampling configurations of the system using the statistical weight. The PI-based reaction free energy introduced by Gillan [23] corresponded to the reversible work of moving the center-of-mass positions (i.e., centroids),

$$\boldsymbol{r}_I^{\rm cent} = \frac{1}{P}\sum_{s=1}^{P}\boldsymbol{r}_I^{(s)}, \quad (3)$$

of the quantum nuclei (ring polymers) along the reaction coordinate [24,26,27,49,50]. First, the MEP and the transition state for H migration in fcc Pd were obtained by using the NEB method [39] in the classical DFT regime. Each of the obtained images along the MEP corresponded to the centroid configuration $\boldsymbol{r}^{\rm cent} = \{\boldsymbol{r}_I^{\rm cent}\}$ of the ring polymers. Then, the path integral average of the centroid force $\boldsymbol{f}(\boldsymbol{r}^{\rm cent})$ was calculated in the canonical ensemble with fixed centroid positions; here, $\boldsymbol{f}(\boldsymbol{r}^{\rm cent})$ is the force acting on the ring polymers when the centroids are located at $\boldsymbol{r}^{\rm cent}$, which is written as

$$\boldsymbol{f}(\boldsymbol{r}^{\rm cent}) = -\nabla^{\rm cent}V_{\rm eff}\left[\left\{\boldsymbol{r}_I^{(s)}\right\}\right] = -\frac{1}{P}\sum_{s=1}^{P}\nabla^{(s)}V\left(\boldsymbol{r}_1^{(s)},\cdots,\boldsymbol{r}_N^{(s)}\right). \quad (4)$$

The PIMD-based free energy profiles were obtained by numerically integrating the centroid mean force along the H-migration path $\boldsymbol{q}$ connecting states X and Y, i.e.,

$$\Delta F(\boldsymbol{q}_Y,\boldsymbol{q}_X) = -\int_{\boldsymbol{q}_X}^{\boldsymbol{q}_Y} d\boldsymbol{q}\cdot\frac{\langle\boldsymbol{f}(\boldsymbol{r}^{\rm cent})\delta(\boldsymbol{r}^{\rm cent}-\boldsymbol{q})\rangle_{\rm PI}}{\langle\delta(\boldsymbol{r}^{\rm cent}-\boldsymbol{q})\rangle_{\rm PI}}, \quad (5)$$

where $\boldsymbol{q}_X$ and $\boldsymbol{q}_Y$ represent the centroid configurations in which the H atom is located either at an O, T, or S site ($X, Y =$ O, T, or S; $X \neq Y$), and δ is Dirac's delta function. We calculated ΔF for H at 150, 300, 450, and 600 K along the path from an O to a T site (O-T path) by fixing the $\boldsymbol{r}^{\rm cent}$ at the images of the original MEP and taking the average of $\boldsymbol{f}(\boldsymbol{r}^{\rm cent})$ over the remaining degrees of freedom. The differences between the free energies of the system $F_{Y\text{-}X}$ for H at different interstitial sites were calculated as $F_{\rm S\text{-}O} \equiv \Delta F(\boldsymbol{q}_{\rm S},\boldsymbol{q}_{\rm O})$, $F_{\rm T\text{-}O} \equiv \Delta F(\boldsymbol{q}_{\rm T},\boldsymbol{q}_{\rm O})$, and $F_{\rm S\text{-}T} \equiv \Delta F(\boldsymbol{q}_{\rm S},\boldsymbol{q}_{\rm T})$. In this analysis, both H and Pd atoms were treated quantum-mechanically by discretizing the imaginary-time path into $P = 12$–32. For each image at each temperature, the PIMD calculations were performed for 1 ps. Hereafter, symbols F and E denote the (free) energies with and without nuclear quantum effects, respectively.

D. H diffusion at the atomic scale

The diffusion coefficient is practically expressed as [1–3]

$$D = D_0 e^{-Q/kT}, \quad (6)$$

where Q is the height of the activation barrier and D_0 is a pre-exponential factor, which is often assumed to be independent of the temperature T. Diffusion at the atomic scale occurs by thermally activated jumps of atoms. Following Wert and Zener [51], the diffusion coefficient of interstitial impurities can be written as

$$D = n\zeta d^2\Gamma, \quad (7)$$

where n is the number of stable nearest-neighbor sites for the diffusing interstitial atom, ζ is the probability that a jump to a nearest-neighbor site leads forward in the diffusion direction, and d is the jump length projected onto the diffusion direction. Γ denotes the jump rate between neighboring sites of the diffusing atom.

If the metastable T interstitial site is sufficiently deep, as is the case for H in Pd, it is reasonable to assume that the diffusing atom temporarily equilibrates at the T site before jumping forward or backward to a neighboring O site. The inclusion of this equilibration leads to the following form of the diffusion coefficient [52,53]:

$$D' = \begin{cases} a^2\Gamma\cdot\frac{1}{2}(1+2e^{-\beta F_{\rm T\text{-}O}})^{-1} & \text{if } F_{\rm T\text{-}O} \geqslant 0 \\ \frac{1}{4}a^2\Gamma\cdot\left(1+\frac{1}{2}e^{\beta F_{\rm T\text{-}O}}\right)^{-1} & \text{otherwise} \end{cases}. \quad (8)$$

This expression is obtained from analyzing the forward and backward steady-state fluxes across the dividing surface, which separates O and T sites. It is assumed that the distribution of H

TABLE I. Convergence tests of classical DFT calculations (without nuclear quantum effects) for H in Pd. a_0 represents the lattice constant at zero stress. $E_{S\text{-}O}$ (or $E_{S\text{-}T}$) is the energy barrier for H migration from an O (or T) site to a T (or O) site via a saddle-point (S) site. $E_{T\text{-}O}$ is the difference between the energies of the system for H in O and T interstitial sites. Note that positive $E_{T\text{-}O}$ value indicates that O sites are favored.

	Functional	E_{cut} (eV)	$\boldsymbol{k}$ points	a_0 (Å)		$E_{S\text{-}O}$ (eV)	$E_{S\text{-}T}$ (eV)	$E_{T\text{-}O}$ (eV)
$Pd_{32}H_1$	GGA-PBE	300	$6 \times 6 \times 6$	3.942 (O site),	3.947 (T site)	0.16	0.11	0.05
	GGA-PBE	400	$16 \times 16 \times 16$	3.945 (O site),	3.948 (T site)	0.16	0.11	0.05
	LDA-CAPZ	300	$6 \times 6 \times 6$	3.847 (O site),	3.850 (T site)	0.27	0.12	0.14
	LDA-CAPZ	400	$16 \times 16 \times 16$	3.845 (O site),	3.848 (T site)	0.25	0.12	0.13
$Pd_{108}H_1$	GGA-PBE	300	$4 \times 4 \times 4$	3.941 (O site),	3.943 (T site)	0.15	0.11	0.04
	GGA-PBE	300	$8 \times 8 \times 8$	3.942 (O site),	3.943 (T site)	0.15	0.11	0.04

atoms between adjacent O and T interstitial sites is governed by a local thermodynamic equilibrium, which is characterized by the difference in the free energy between H at O and T sites, $F_{T\text{-}O}$. It is noted that the isotropic diffusivity for an O-T network in the fcc lattice without correlation [54] can be reduced to Eq. (8), when one neglects the difference in the jump frequencies of the solvent atom at the O and T sites.

III. RESULTS AND DISCUSSION

A. H migration in strained Pd

The MEP and the transition state of H migration along the path between the neighboring O sites via the intermediate T site (i.e., O-T-O hopping) were obtained using the NEB method based on DFT for a $Pd_{32}H$ supercell at 3.1 at.% H. The difference between the energies of the system for H in O and T sites is defined as $E_{T\text{-}O}$. Note that a positive $E_{T\text{-}O}$ value indicates that the O site is energetically favorable. Another special site is the saddle-point (S) site located near the midpoint between the O and the T sites. We define the energy of the S site relative to that of the O and T sites as $E_{S\text{-}O}$ and $E_{S\text{-}T}$, respectively.

Table I gives the convergence properties of the classical DFT-NEB calculations with respect to the energy cutoff (E_{cut}) and $\boldsymbol{k}$-point mesh, using the LDA and GGA functionals. We find that a relatively modest E_{cut} (300 eV) and $\boldsymbol{k}$-point mesh ($6 \times 6 \times 6$) produce converged energetic results. An additional test using a $Pd_{108}H$ supercell with dimensions of $3a \times 3a \times 3a$ shows that the energies are almost converged with respect to cell size. Further, the GGA functional provides a more accurate and consistent picture of the energetics of the Pd-H system than the LDA functional through the excellent agreement with the experimental value of the H-diffusion barrier [1] when nuclear quantum effects are properly considered (see Appendix A). Thus our discussion in the remainder of this study is based on the results from the GGA-PBE functional with a E_{cut} of 300 eV and a $6 \times 6 \times 6$ $\boldsymbol{k}$-point mesh.

To investigate the effects of elastic strain on the site energetics and intermigration of H in Pd, MEPs were calculated in the strained lattice for several values of the magnitude of the hydrostatic (i.e., homogeneous triaxial) tensile strain, which is defined as $\epsilon_h = a/a_0 - 1$, where a and a_0 represent the lattice constants in the current and reference configurations, respectively. The four values of 0.6%, 1.2%, 1.8%, and 2.4% were chosen as ϵ_h; positive values of ϵ_h correspond to lattice expansion in this definition. The supercell in the reference configuration was deformed with every ϵ_h, and then only the atomic coordinates were allowed to relax. Note that, because of the lattice symmetry, the O and T interstitial sites in the regular Pd lattice remain equivalent for arbitrary homogeneous strains.

In Fig. 1, we show the strain-dependent MEPs of the H atom moving between the O (left and right) and the T (middle) sites via the S sites in the fcc Pd lattice. The DFT result shows that the H atom is stable at the O site for unstrained Pd; the H-migration barrier (i.e., $E_{S\text{-}O}$) in Pd is equal to 0.16 eV. This value excludes the nuclear quantum effects and thus corresponds to the "classical" limit of the barrier, as discussed in Sec. III B and Appendix A. The shape of MEP for H migration drastically changes with ϵ_h, as shown in Fig. 1. Even for small strains, the migration barrier decreases monotonically as the strain is increased, reaching the minimum of 0.10 eV at $\epsilon_h = 1.2\%$. It is interesting to see that the $E_{T\text{-}O}$ steadily decreases as ϵ_h is increased; furthermore, the H atom at the T site becomes more energetically stable than that at the O site under large strains ($>1.2\%$). In such situations, the $E_{S\text{-}T}$ value becomes dominant for the activation of H migration along the O-T path, instead of the $E_{S\text{-}O}$. Consequently, the H-migration barrier along the O-T path is decreased by 39% at $\epsilon_h = 2.4\%$.

B. Nuclear quantum effects on H migration

It is important to use a sufficient number of beads in the PIMD calculations to accurately capture the nuclear quantum effects of interest. During the convergence tests, we noted the root-mean-square radius of gyration (R_g), which describes the dispersion of the H nucleus and is thus an important indicator of the extent of quantum nuclear delocalization (as discussed in Sec. III C). We calculated the mean value of the R_g of the H

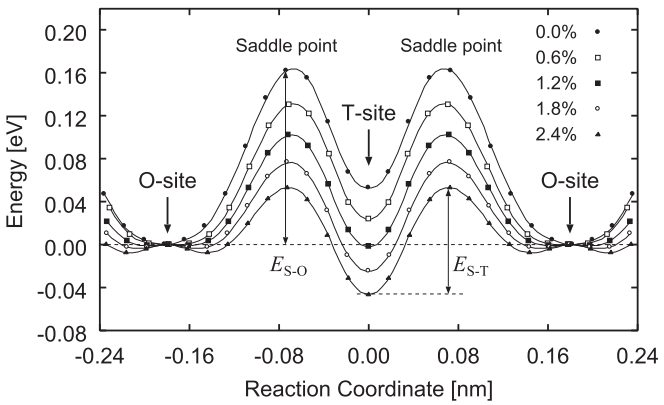

FIG. 1. Minimum-energy paths for H migration in Pd for different hydrostatic strains.

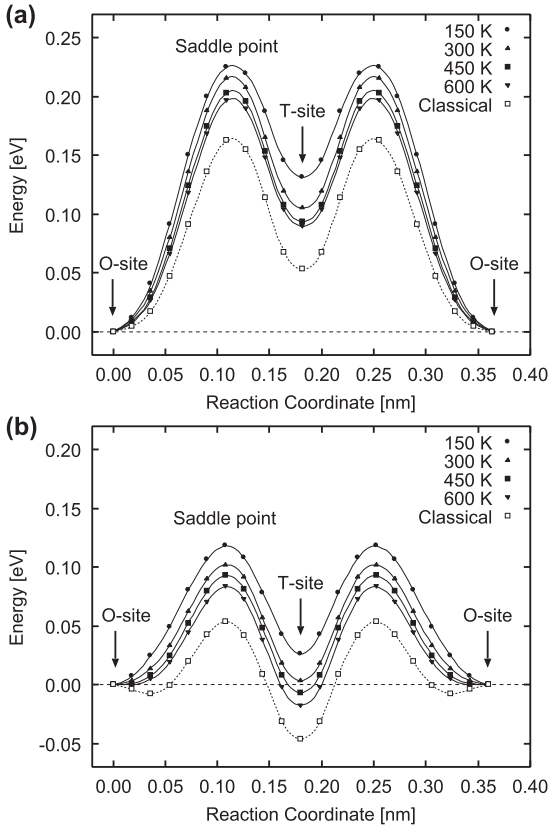

FIG. 2. Free energy profiles for H migration in Pd along the O-T-O path at various temperatures: (a) profiles at $\epsilon_h = 0.0\%$ and (b) profiles at $\epsilon_h = 2.4\%$.

atom at the most stable interstitial site (i.e., the O site) during the 1-ps run and obtained 0.140 Å for $P = 12$ and 0.137 Å for $P = 32$ at 150 K; the value of R_g when using 32 beads is only a few percent smaller than that when using 12 beads, even at the lower end of the temperature range considered. The tests show that 12 beads provide a good compromise between accuracy and computational cost for the properties of H delocalization in this system.

The PIMD-based free energy profiles for H migration between the O and T sites in unstrained Pd are evaluated at 150–600 K, as shown in Fig. 2(a). We confirm that the H-migration barrier (i.e., $F_{S\text{-}O}$) dramatically increases as the temperature is decreased. The $F_{S\text{-}O}$ values at the relatively low temperatures of 150 and 300 K are calculated as 0.23 and 0.22 eV, respectively, lying between the classical DFT value of 0.16 eV and the zero-point energy (ZPE)-corrected DFT value of 0.27 eV (see Appendix B). In addition, the difference between the free energies of the H atom at the O and T sites ($F_{T\text{-}O}$) also increases as the temperature is decreased; the $F_{T\text{-}O}$ values at 150 and 300 K are 2.5 and 2.0 times larger, respectively, than that of the classical limit. This indicates that the quantum effects hinder the accessibility of the O-T migration path at lower temperatures. It is noteworthy that the nuclear quantum effects are manifested even at relatively high temperatures; the $F_{S\text{-}O}$ and $F_{T\text{-}O}$ at 600 K are increased by 21% and 69%, respectively, relative to the classical limit. This suggests that the quantum nature of H nuclei is essential for understanding the H-diffusion kinetics in Pd over the entire temperature range of 150–600 K.

We investigated the H migration in strained Pd lattices, in which nuclear quantum effects at finite temperatures (150–600 K) were considered. The free energy profiles for H migration under $\epsilon_h = 2.4\%$ are shown in Fig. 2(b). The hydrostatic strain significantly changes the shape of the profile, induced by both the internal relaxation of the atomic positions and the resultant modification of nuclear quantum effects. The results show that the H diffusivity in strained Pd is dominated by the combination of the competing effects of quantum fluctuations and lattice expansion: the activation barrier for H migration is significantly increased with decreasing temperature while it is drastically decreased with increasing hydrostatic strain. Further, although the classical DFT results show that the T site becomes increasingly more stable than the O site with lattice expansion, the PIMD results indicated that this reduction in energy is largely compensated by the nuclear quantum effects arising from the difference between curvatures of the potential surface (i.e., degrees of confinement of the H nucleus) at the O and T sites. Consequently, in the studied range of hydrostatic strains, the state of the H atom located at the O site exhibits the lowest free energy over a wide temperature range, except at high strain and/or high temperature. This tendency may be decreased for heavier isotopes of H and/or for higher temperatures because of the decreased contribution of nuclear quantum effects.

In addition, it is noted that the O site becomes unstable at $\epsilon_h = 2.4\%$ such that the minimum basins are formed around the O site at a distance of 0.36 Å from the O site toward the T site due to the symmetry breaking, as in Fig. 1. However, the PIMD results indicated that the difference between the energies of the system for H in O and basin sites is sufficiently small (∼8 meV) so that the basins become negligible in the free energy surface due to the nuclear quantum effects. Eventually, H atoms tend to prefer the original O sites with enlarged free volume to the basin sites, as shown in Fig. 2(b).

The temperature and strain dependence of the $F_{S\text{-}O}$, $F_{S\text{-}T}$, $F_{T\text{-}O}$, and the activation free energy for H migration F_m for H in Pd are summarized in Fig. 3. Here, it is noted that the F_m is described as $\max(F_{S\text{-}O}, F_{S\text{-}T})$. In Fig. 3, the $F_{S\text{-}O}$ and $F_{T\text{-}O}$ decrease almost linearly with respect to ϵ_h in a similar manner at any temperature condition. On the contrary, $F_{S\text{-}T}$ changes little over the entire strain range of 0.0%–2.4%, regardless of temperature. It is interesting to see that this leads to the crossover of dominant activation barriers for H migration along the O-T path; the contribution of $F_{S\text{-}T}$ overcomes that of $F_{S\text{-}O}$ with increasing strain. The results indicate that, when the O site is preferred for the H atom under small strains, the $F_{S\text{-}O}$ tends to increase significantly with decreasing temperature owing to the nuclear quantum effects. In contrast, as the T site becomes progressively more stable with lattice expansion, the nuclear quantum effects become less prominent and no longer inhibit the H migration (namely, temperature has little effect on the $F_{S\text{-}T}$). In other words, the strain-dependent diffusion mechanism for O-T-O hopping has a prominent quantum nature until it switches to a classical-like T-O-T hopping (between neighboring T sites via a metastable O site) at the strain of ∼2.4%. Consequently, the F_m approaches the lower bound of approximately 0.10 eV as ϵ_h is increased, as displayed

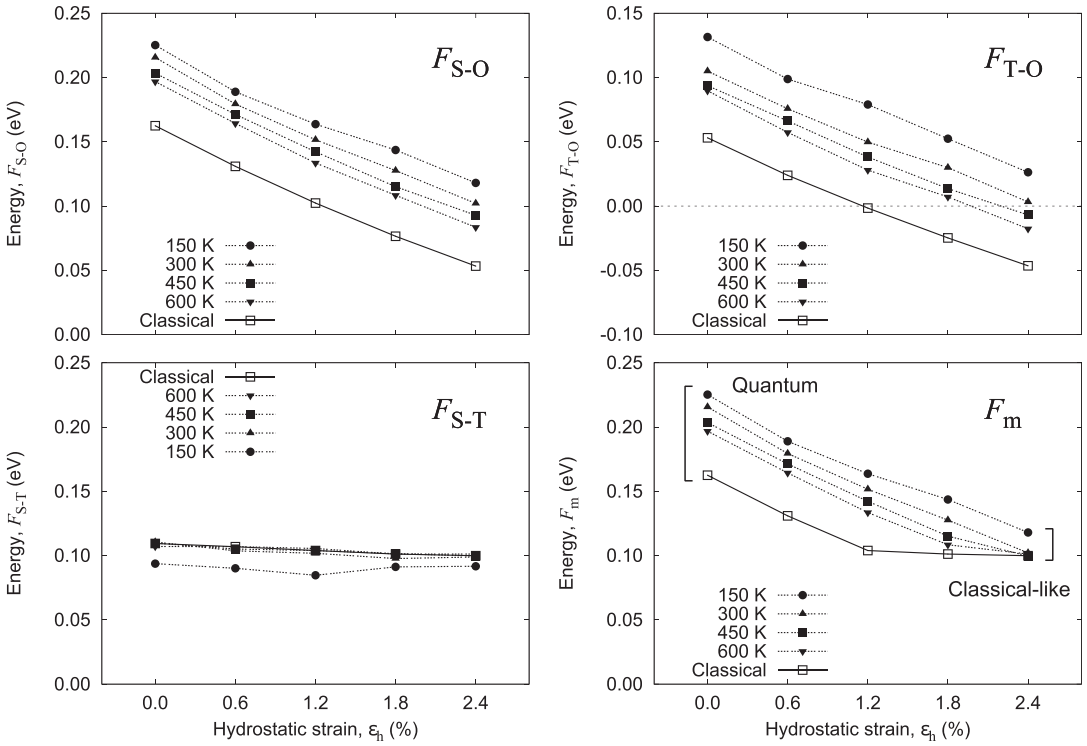

FIG. 3. Temperature and strain dependence of the $F_{S\text{-}O}$, $F_{S\text{-}T}$, $F_{T\text{-}O}$, and F_m [i.e., $\max(F_{S\text{-}O}, F_{S\text{-}T})$] of H in Pd.

in Fig. 3. The H migration in such a situation is expected to serve as a fast diffusion mechanism where the $F_{S\text{-}T}$ is dominant.

In this study, the centroid intrinsic reaction coordinates (IRCs) were assumed to correspond to the classical MEP, to avoid the huge computational costs required for the optimization of centroid IRCs. Such an approximation is typically valid for the semiclassical regime. On the other hand, if the positions of the minimum and saddle points of the centroid free energy surface are near to those of the classical counterpart, then one can anticipate that the approximation of centroid free energy difference on the classical MEP will be valid. To test this view, we decomposed the PIMD-based free energy gradient (i.e., centroid mean force) at the minimum and saddle points into components parallel and perpendicular to the classical MEP, and then checked the magnitude of the perpendicular component that may lead to deviation from the original (i.e., classical) path. As a result, we confirmed that the absolute value of each perpendicular component of the centroid mean force is 18 meV/Å in average and does not exceed 34 meV/Å even at the lower end of the temperature range considered. Since these values are comparable to the typical values of force tolerance for structural relaxation, it is unlikely that the residual centroid force perpendicular to the path significantly alters the dominant process of the H diffusion. This probably stems from the fact that the H-diffusion process in fcc Pd intrinsically has a large activation barrier in the classical limit (∼0.16 eV) and a relatively long hopping distance for the H atom between the O and T sites (∼1.7 Å), which retains its integrity regardless of presence of quantum effects over the temperature range of 150 to 600 K.

The approach we used can capture the quantum mechanical effects at low temperatures while seamlessly transitioning to the classical limit at high temperatures. We should note that the temperature range considered (150–600 K) is intermediate between the quantum and classical regimes. We performed additional tests in a wide temperature range (75–1200 K) based on the same approach and confirmed a smooth and consistent transition between the two regimes (see Ref. [55]). Our results and the results of Di Stefano *et al.* [56] suggest a possibility that the quantum effects can influence the H diffusion in fcc metals even at high temperatures (∼1000 K) due to the strong confinement of the H atom along its migration path. Nuclear quantum effects tend to remain at high temperature in systems with relatively stiff bonds, such as water vapor [57], diamond [58], and graphene [59,60], which lead to gradual convergence of structural and thermal properties to their classical limits.

C. Quantum distribution of a H atom

To investigate the state of a H atom in Pd, three centroid positions for T, S, and O sites were considered. Figure 4 shows the quantum distributions of the ring polymer representing the H atom at different temperatures. At a high temperature of 600 K, the H-atom distribution at all sites is confined and almost isotropic on the (001) plane. On the other hand, at 150 K, the distribution at the S site broadens substantially and is spread between the O and T sites (parallel to the O-T path). Further, the distribution at the O site indicates a relatively large uncertainty in the position of the H atom. These facts suggest that such intersite migrations are influenced by the temperature-dependent quantum delocalization of the H atom.

The size of the ring polymer is characterized by the root-mean-square radius of gyration R_g, which is defined as

$$(R_g)^2 = \frac{1}{P}\left\langle \sum_{s=1}^{P} (r^{(s)} - r^{\text{cent}})^2 \right\rangle_{\text{PI}}, \tag{9}$$

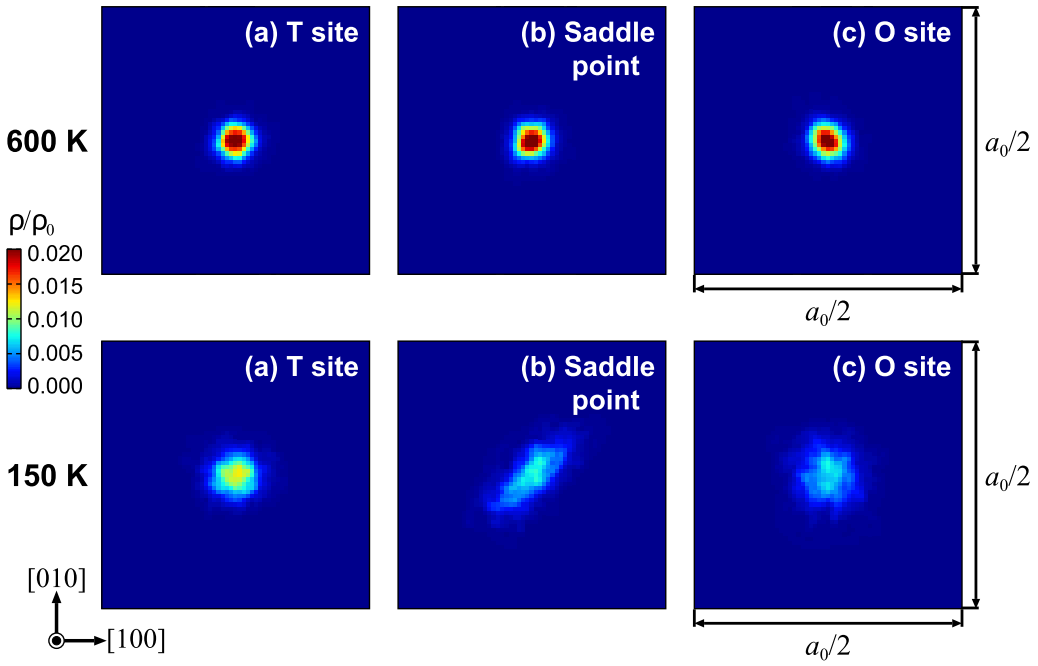

FIG. 4. Quantum distribution of the H atom in Pd at different temperatures, i.e., at 600 K (top) and 150 K (bottom). At each temperature, the results are shown with the centroid of the H atom located at the (a) T site, (b) saddle-point S site, and (c) O site.

where r^{cent} is the instantaneous one-dimensional centroid of the ring polymer. For free particles with a mass of m, in the limit $P \to \infty$ [23],

$$\left(R_{\text{g}}^{\text{fp}}\right)^2 = \hbar^2/(12mkT) = \pi\Lambda^2/6, \tag{10}$$

where Λ denotes the thermal de Broglie wavelength. If the quantum particle is confined by a potential, then the low-temperature spreading is limited, and R_{g} approaches a constant for $T \to 0$. This can be examined analytically for the harmonic oscillator, for which in the $P \to \infty$ limit [23],

$$(R_{\text{g}}^{\text{ho}})^2 = \frac{kT}{m\omega_0^2}\left[\frac{\hbar\omega_0}{2kT}\coth\left(\frac{\hbar\omega_0}{2kT}\right) - 1\right], \tag{11}$$

where ω_0 is the oscillator frequency.

We calculated the three orthogonal components of R_{g}'s of the quantum distributions of the H atom about the principal axes of inertia (Fig. 5). They are nearly degenerate for the O and T sites because of the cubic symmetry of the sites in the fcc lattice, while those for the S site show a significant difference between the components parallel ($\parallel$) and perpendicular ($\perp$) to the H-migration path, as illustrated in Fig. 4(b). Especially, the quantum distribution of the H atom parallel to the path is significantly spread beyond the free-particle limit, while those perpendicular to the path are localized to the same degree at the T site because of the relatively strong confinement. For the O and T sites, the *effective* vibrational energy $\hbar\omega_0$ is obtained by fitting Eq. (11) to the R_{g} as a function of ω_0. The obtained values are $\hbar\omega_0 = 65$ meV for O sites and 146 meV for T sites at $\epsilon_{\text{h}} = 0.0\%$. Notably, the value for the O site at zero strain agrees with previously reported experimental values of 62.4–69 meV [9,61]. This indicates that the anharmonicity of the potential surface around the H-preferred site (i.e., the O site) is effectively incorporated in the present *ab initio* PIMD calculations by sampling the delocalized states of the H atom. We obtained $\hbar\omega_0 = 52$ meV for the O site and 122 meV for the T site at $\epsilon_{\text{h}} = 2.4\%$. The decrease in $\hbar\omega_0$ with respect to ϵ_{h} is attributed to a local lattice relaxation at and around the O and T sites, which causes a reduction in the curvature of the potential surface and in the degree of confinement of the H atom.

D. Diffusion coefficients

Although the PIMD calculation can provide F_{m} according to the Eq. (5), the direct evaluation of Γ of the H jump is difficult using only the PIMD result. Γ is described by the transition state theory (TST) as

$$\Gamma = \nu_0 e^{-\beta F_{\text{m}}}, \quad F_{\text{m}} = \max(F_{\text{S-O}}, F_{\text{S-T}}), \tag{12}$$

where ν_0 represents the jump frequency of the H atom along the diffusion path [62]. In this study, ν_0 was approximated as the frequency of oscillation of the H atom in the q direction and roughly estimated from a harmonic fit to the energy along the corresponding reaction coordinate determined by classical DFT-NEB calculations. As a result, the values were obtained as $\nu_0 = 7.9$, 6.2, and 4.7 (in THz) at the hydrostatic strains of 0.0%, 1.2%, and 2.4%, respectively. The harmonic estimates are expected to be valid when the reduced barrier height is sufficiently large ($\beta F_{\text{m}} \gg 1$) [63].

Figure 6 shows the computed jump rates [i.e., Γ in Eq. (12)] of the H atom from the O to T site in unstrained Pd as a function of inverse temperature. To characterize the change in Γ over a wide temperature range, the PIMD results at 75, 100, 900, and 1200 K (see Ref. [55]) are also plotted in Fig. 6. While the rate is confirmed to approach the classical limit (i.e., $\nu_0 e^{-\beta E_{\text{S-O}}}$) at high temperatures, a deviation from the linear behavior with decreasing temperature is observed, which is attributed to the significant increase in the $F_{\text{S-O}}$ with decreasing temperature owing to nuclear quantum effects. Further, a turn-up in the

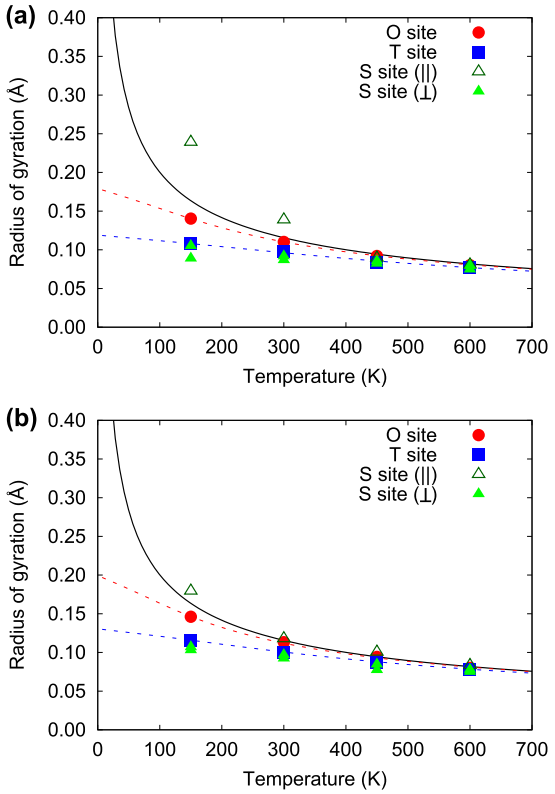

FIG. 5. Temperature dependence of the radius of gyration (R_g) of a ring polymer representing the H atom located at the O, T, and S sites in Pd: (a) results at $\epsilon_h = 0.0\%$ and (b) results at $\epsilon_h = 2.4\%$. Dotted curves represent the fitting results based on the harmonic oscillator approximation [Eq. (11)]: (a) $\hbar\omega_0 = 65$ meV for O site and 146 meV for T site at $\epsilon_h = 0.0\%$ and (b) $\hbar\omega_0 = 52$ meV for O site and 122 meV for T site at $\epsilon_h = 2.4\%$. The solid curve represents the free-particle limit [Eq. (10)].

rate becomes prominent at low temperatures below 150 K due to the onset of quantum tunneling. This indicates that the approach we used can capture a seamless transition between the classical and quantum regimes. The temperature range considered in this study (namely, 150–600 K) is intermediate between the two regimes.

According to the Eqs. (8) and (12), the diffusion coefficients of interstitial H in Pd were predicted based on the PIMD values of F_m and $F_{T\text{-}O}$. Figure 7 shows the Arrhenius plots of the diffusion coefficients of H in fcc Pd at hydrostatic strains of 0.0%–2.4% in the temperature range of 150–600 K. For comparison, the experimental D values from Refs. [11,64–66] are also plotted in Fig. 7. In addition, the D' values estimated from Eyring's TST [67] using the DFT-calculated energies with and without ZPE correction, which include the effects of local equilibration in the metastable site according to the Eq. (8), are drawn as curves in Fig. 7. (Details are described in Appendix B.) In the PIMD results, the logarithmic D' value appears to vary linearly with the inverse temperature; however, the curve is actually concave down in this temperature range because of the significant change in F_m with respect to temperature, as found in Fig. 3. In Fig. 7, our PIMD results are in reasonable agreement with experimental measurements over a wide temperature range. Although this agreement should not

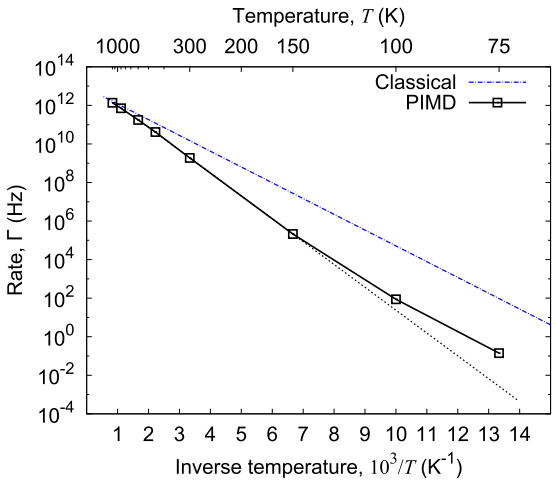

FIG. 6. Jump rates of the H atom from the O to T site in unstrained Pd in the temperature range 75–1200 K. Plots represent the PIMD results and the dotted line is an Arrhenius fit of the data in the intermediate temperature range 150–600 K: $\Gamma(T) = 1.71\times10^{13}\exp(-0.235\ \text{eV}/kT)$ Hz. The dashed-dotted line represents the classical limit.

be overemphasized because of the rough approximation of ν_0 made in the TST-based model calculations, it does indicate that our *ab initio* modeling is to the point.

In several experimental studies, the Q values were practically estimated by the slope of ln D versus $1/T$ plot between 213 and 1373 K [1,11,64–66], as listed in Table II. For comparison with these results, we evaluated the slope and intercept of the PIMD-based D' values by linear approximation over the temperature range of 150–600 K. The obtained Q and D_0 values are also listed in Table II. The PIMD-based Q value of 0.23 eV at $\epsilon_h = 0.0\%$ shows excellent agreement with the experimental data [1,11,64–66] for unstrained bulk

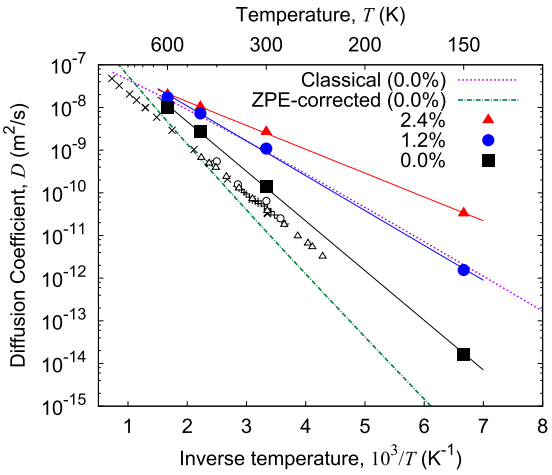

FIG. 7. Diffusion coefficients of H in Pd in the temperature range 150–600 K. Solid plots represent the PIMD results and the lines are Arrhenius fits of the data: $D(T) = D_0\exp(-Q/kT)$. The obtained Q and D_0 values are listed in Table II. The experimental data are taken from Refs. [11,64–66]; open circles [11], cross symbols [64], plus symbols [65], and open triangles [66]. The dotted and dashed-dotted curves represent classical [Eq. (B2)] and ZPE-corrected [Eq. (B3)] DFT results, respectively.

TABLE II. Calculated values for apparent activation barrier (Q) and pre-exponential factor (D_0) of H diffusivity in fcc Pd in the temperature (T) range of 150–600 K, together with experimental values. The PIMD and DFT results are obtained using the GGA-PBE functional.

	Q (eV)	D_0 (10^{-7} m^2 s^{-1})	T range (K)
PIMD ($\epsilon_h = 0.0\%$)	0.23	9.9	150–600
PIMD ($\epsilon_h = 1.2\%$)	0.16	4.6	150–600
PIMD ($\epsilon_h = 2.4\%$)	0.11	1.8	150–600
Classical DFT[a]	0.15	3.2	150–600
ZPE-corrected DFT[a]	0.30	13.3	150–600
Expt. (Ref. [1])	0.23	2.9	230–900
Expt. (Ref. [11])	0.23	5	280–400
Expt. (Ref. [64])	0.238	3.512	298–1373
Expt. (Ref. [65])	0.228	3.09	273–353
Expt. (Ref. [66])	0.226	2.5	213–473

[a]At $\epsilon_h = 0.0\%$ [see Eqs. (B2) and (B3) in Appendix B].

Pd. On the other hand, the corresponding D_0 value of 9.9 (in 10^{-7} m^2 s^{-1}) is somewhat overestimated compared with the experimental values ranging from 2.5 to 5 (in 10^{-7} m^2 s^{-1}) [1,11,64–66]. Because the classical limit for the migration barrier (i.e., E_m) on the DFT-based potential energy surface is 0.16 eV, the apparent Q is confirmed to increase by 44% when nuclear quantum effects are considered. This confirms that the H diffusivity in the quantum regime is much slower than that in the classical one. This view is consistent with experimental measurements concerning the *reversed* isotope dependence for H diffusion in Pd [1,3,66], which implies that heavier isotopes of H exhibit smaller activation energies for lattice diffusion. On the other hand, the ZPE-corrected DFT result exhibits the apparent Q value of 0.30 eV, which strongly deviates from not only those in the experimental measurements but also the PIMD-based value. This indicates that the temperature-dependent nature of the activation barrier and/or pre-exponential factor is essential to characterize the H diffusivity in fcc Pd.

As suggested in Fig. 3, the hydrostatic tensile strain can induce the fast motion of H in the Pd lattice with changes in the free energy landscape for H migration. We confirm that both Q and D_0 apparently decrease as ϵ_h is increased, as in Fig. 7 and Table II. In particular, it is noteworthy that the fast lattice diffusion at $\epsilon_h = 2.4\%$ of H ($Q = 0.11$ eV) is predicted to occur, approximately 20 times faster than the conventional H diffusion ($Q = 0.23$ eV) in unstrained Pd at a room temperature of 300 K. Our *ab initio* results indicated that the H diffusivity in Pd is dramatically influenced by a hydrostatic tensile strain on the order of 1%–2%, which accompanies a change of the H-preferred site (from the O site to T site) and the resultant reduction of nuclear quantum effects.

IV. CONCLUSIONS

The migration kinetics and diffusivity of H in fcc Pd were investigated by performing *ab initio* PIMD modeling in the framework of DFT. We determined that the fcc Pd lattice permitted a mechanism for the fast lattice diffusion of interstitial H with the help of lattice expansion, which accompanies a change in H atom preference between the two interstitial sites (i.e., the O and T sites). The nuclear quantum effects tended to assist the conventional O-T-O hopping and inhibit the T-O-T hopping that is enhanced under the hydrostatic tensile strain. Generally, the free energy profiles for H migration in metals at finite strains were sensitive to the underlying potential-energy surface and therefore could not be properly analyzed without using the *ab initio* approach based on reliable electronic-structure calculations. The present analysis that explicitly included the quantum mechanical nature of both electrons and nuclei was effective to handle this issue and provided a deep insight for understanding temperature-dependent H-diffusion behaviors in the Pd lattice. The elucidated mechanism for the interplay of the quantum effects and lattice strain may serve as relevant information for the design and exploitation of advanced Pd-based nanomaterials for H permeation and/or storage; this finding may allow exploration of the concept of "strain-field design" for H permeation and storage materials, utilizing the intrinsic elastic strain fields induced around nanostructured defects, such as large-misfit heterophase interfaces, solute-segregated grain boundaries, and chemically heterogeneous surfaces.

ACKNOWLEDGMENTS

H.K. and S.O. appreciate the support from the Elements Strategy Initiative for Structural Materials (ESISM) from the Ministry of Education, Culture, Sports, Science and Technology (MEXT), Japan.

APPENDIX A: LDA VERSUS GGA CALCULATIONS

To check the influence of the exchange-correlation functional on the present results, the MEP and free energy profile (at 300 K) for H migration in Pd were calculated using the LDA functional, as well as using the GGA-PBE functional as described in Sec. III B. The LDA functional used here was given by Ceperley and Alder [37] and parametrized by Perdew and Zunger [38] (CAPZ). In Fig. 8, the classical DFT results (open plots) of the H-migration barrier show a significant difference between the two functionals, i.e., $E_{S\text{-}O} = 0.27$ eV for LDA-CAPZ and $E_{S\text{-}O} = 0.16$ eV for GGA-PBE (the energies are listed in Table I). Because the experimental value of the H-diffusion barrier in unstrained bulk Pd is approximately 0.23 eV [1], one may conclude that the CAPZ functional provides a relatively good result for the energetics of the H-diffusion process in Pd, in which the classical activation barrier is closer to the experimental value than that calculated using the PBE functional. However, if one takes the PIMD calculation with the inclusion of nuclear quantum effects, the barrier heights are effectively increased for both functionals (solid plots). Consequently, the F_m obtained using the PBE functional (0.22 eV) is in excellent agreement with the experimental value of 0.23 eV, whereas that using the CAPZ functional (0.31 eV) is apparently overestimated. Since a critical term in the diffusivity is the effective height of the diffusion barrier, such an overestimation of F_m in the LDA-CAPZ calculations can lead to large systematic errors in quantitative analysis. Actually, the PIMD-based D' value [according to the Eqs. (8) and (12)] at 300 K when using the LDA-CAPZ functional is estimated to be 27.2 times smaller than that when using

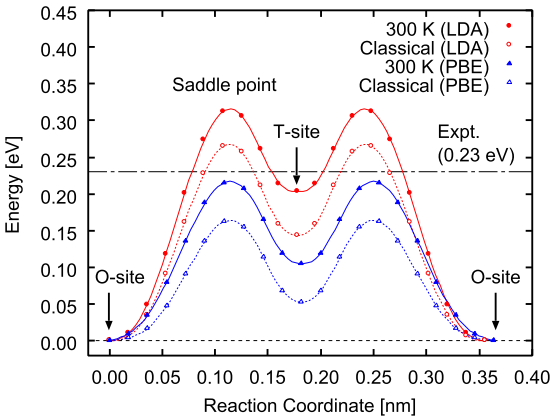

FIG. 8. Minimum-energy paths and corresponding free energy profiles (300 K) for interstitial H migration in Pd obtained using the LDA and GGA functionals. Open and solid plots represent the classical DFT and PIMD results, respectively. The dashed-dotted line corresponds to the representative value of the activation barrier for H diffusion in bulk Pd obtained from the best fit to the experimental D values reported in different studies [1].

the GGA-PBE functional. We conclude that the GGA-PBE calculations provide more accurate and consistent pictures of the energetics of the Pd-H system than those from the LDA-CAPZ calculations. This view is also supported by the fact that the experimental diffusion barriers of *heavier* isotopes of H in Pd (0.206 eV for D and 0.186 eV for tritium) [66,68] are *closer* to the classical limit ($E_{\text{S-O}} = 0.16$ eV) obtained using the PBE functional. Thus our discussion in this article is based on the results from the GGA-PBE functional.

APPENDIX B: EYRING'S TST

Following Eyring's theory of the activated complex [67], the mean velocity for crossing the transition state is taken from the velocity distribution of classical particles at T. The jump rate is given by

$$\Gamma = \frac{kT}{h}\frac{Z^{\ddagger}}{Z^{0}} e^{-E_{\text{m}}/kT}, \tag{B1}$$

where $Z^{\ddagger}$ and Z^{0} are partition functions for the transition and ground states, respectively, and h is the Planck constant (i.e., $h = 2\pi\hbar$).

Within the harmonic approximation of Eq. (B1), the jump rate for the high-temperature range is described as

$$\Gamma_{\text{cl}} = \frac{\prod_{i=1}^{3N-3} \nu_i^0}{\prod_{i=1}^{3N-4} \nu_i^{\ddagger}} e^{-E_{\text{m}}/kT} = \nu^* e^{-E_{\text{m}}/kT}, \tag{B2}$$

where $\nu_i^{\ddagger}$ and ν_i^0 are the real nonzero vibrational frequencies in the transition and ground states, respectively. Similarly, the jump rate for the low-temperature range is written as

$$\begin{aligned}\Gamma_{\text{qm}} &= \frac{kT}{h}\frac{\exp\sum_{i=1}^{3N-3}\frac{h\nu_i^0}{2kT}}{\exp\sum_{i=1}^{3N-4}\frac{h\nu_i^{\ddagger}}{2kT}} e^{-E_{\text{m}}/kT} \\ &= \frac{kT}{h} e^{-(E_{\text{m}}+\Delta E_{\text{zp}})/kT},\end{aligned} \tag{B3}$$

where ΔE_{zp} $(= \sum_i \frac{1}{2}h\nu_i^{\ddagger} - \sum_i \frac{1}{2}h\nu_i^0)$ is the difference in ZPEs between the ground and transition states.

The Hessian matrix and vibrational frequencies ν_i of the system were determined from the forces acting on atoms within the classical DFT regime, in which each atom was displaced (by ± 0.01 Å) in the direction of each Cartesian coordinate. The obtained ZPE-corrected energies are (in eV) $E_{\text{S-O}}^{\text{zp}} = 0.27$ (0.24–0.31) [17,20] and $E_{\text{T-O}}^{\text{zp}} = 0.18$ (0.16) [17], where the numbers in parentheses are the previously reported DFT results within the GGA [17,20]. This indicates that our computational settings are sufficiently compatible with the previous DFT calculations.

[1] J. Völkl and G. Alefeld, in *Hydrogen in Metals I: Basic Properties*, edited by G. Alefeld and J. Völkl, Topics in Applied Physics Vol. 28 (Springer, Berlin, 1978), pp. 321–348.
[2] H. Wipf, in *Hydrogen in Metals III: Properties and Applications*, edited by H. Wipf, Topics in Applied Physics Vol. 73 (Springer, Berlin, 1997), pp. 51–91.
[3] Y. Fukai, *The Metal-Hydrogen System: Basic Bulk Properties*, 2nd ed. (Springer, Berlin, 2005).
[4] S. N. Paglieri and J. D. Way, Sep. Purif. Methods **31**, 1 (2002).
[5] J. J. Conde, M. Maroño, and J. M. Sánchez-Hervás, Sep. Purif. Rev. **46**, 152 (2017).
[6] T. Mütschele and R. Kirchheim, Scr. Metall. **21**, 135 (1987).
[7] U. Stuhr, T. Striffler, H. Wipf, H. Natter, B. Wettmann, S. Janssen, R. Hempelmann, and H. Hahn, J. Alloys Compd. **253-254**, 393 (1997); S. Janßen, H. Natter, R. Hempelmann, T. Striffler, U. Stuhr, H. Wipf, H. Hahn, and J. C. Cook, Nanostruct. Mater. **9**, 579 (1997).
[8] H. Iwaoka, M. Arita, and Z. Horita, Acta Mater. **107**, 168 (2016).
[9] M. Kofu, N. Hashimoto, H. Akiba, H. Kobayashi, H. Kitagawa, M. Tyagi, A. Faraone, J. R. D. Copley, W. Lohstroh, and O. Yamamuro, Phys. Rev. B **94**, 064303 (2016).
[10] H. Akiba, M. Kofu, H. Kobayashi, H. Kitagawa, K. Ikeda, T. Otomo, and O. Yamamuro, J. Am. Chem. Soc. **138**, 10238 (2016).
[11] B. J. Heuser, D. R. Trinkle, N. Jalarvo, J. Serio, E. J. Schiavone, E. Mamontov, and M. Tyagi, Phys. Rev. Lett. **113**, 025504 (2014).
[12] E. J. Schiavone and D. R. Trinkle, Phys. Rev. B **94**, 054114 (2016).
[13] J. Weissmüller and C. Lemier, Phys. Rev. Lett. **82**, 213 (1999).
[14] V. P. Zhdanov and B. Kasemo, Nano Lett. **9**, 2172 (2009).
[15] B. Baranowski, S. Majchrzak, and T. B. Flanagan, J. Phys. F: Met. Phys. **1**, 258 (1971).
[16] B. Ingham, M. F. Toney, S. C. Hendy, T. Cox, D. D. Fong, J. A. Eastman, P. H. Fuoss, K. J. Stevens, A. Lassesson, S. A. Brown, and M. P. Ryan, Phys. Rev. B **78**, 245408 (2008).
[17] P. Kamakoti and D. S. Sholl, J. Membr. Sci. **225**, 145 (2003).
[18] S. Hong and T. S. Rahman, Phys. Rev. B **75**, 155405 (2007).
[19] O. Y. Vekilova, D. I. Bazhanov, S. I. Simak, and I. A. Abrikosov, Phys. Rev. B **80**, 024101 (2009).
[20] H. Grönbeck and V. P. Zhdanov, Phys. Rev. B **84**, 052301 (2011).
[21] C. Zhang and A. Michaelides, Surf. Sci. **605**, 689 (2011).

[22] R. P. Feynman and A. R. Hibbs, *Quantum Mechanics and Path Integrals* (McGraw-Hill, New York, 1965).

[23] M. J. Gillan, Phys. Rev. Lett. **58**, 563 (1987); Philos. Mag. A **58**, 257 (1988).

[24] G. Mills and H. Jónsson, Phys. Rev. Lett. **72**, 1124 (1994).

[25] M. Leino, J. Nieminen, and T. T. Rantala, Surf. Sci. **600**, 1860 (2006).

[26] H. Kimizuka, H. Mori, and S. Ogata, Phys. Rev. B **83**, 094110 (2011).

[27] H. Kimizuka and S. Ogata, Phys. Rev. B **84**, 024116 (2011).

[28] T. Yoshikawa, T. Takayanagi, H. Kimizuka, and M. Shiga, J. Phys. Chem. C **116**, 23113 (2012).

[29] E. M. McIntosh, K. T. Wikfeldt, J. Ellis, A. Michaelides, and W. Allison, J. Phys. Chem. Lett. **4**, 1565 (2013).

[30] I. H. Katzarov, D. L. Pashov, and A. T. Paxton, Phys. Rev. B **88**, 054107 (2013).

[31] G. Kyriakou, E. R. M. Davidson, G. Peng, L. T. Roling, S. Singh, M. B. Boucher, M. D. Marcinkowski, M. Mavrikakis, A. Michaelides, and E. C. H. Sykes, ACS Nano **8**, 4827 (2014).

[32] R. Quhe, M. Nava, P. Tiwary, and M. Parrinello, J. Chem. Theory Comput. **11**, 1383 (2015).

[33] G. Kresse and J. Furthmüller, Phys. Rev. B **54**, 11169 (1996).

[34] P. E. Blöchl, Phys. Rev. B **50**, 17953 (1994).

[35] G. Kresse and D. Joubert, Phys. Rev. B **59**, 1758 (1999).

[36] J. P. Perdew, K. Burke, and M. Ernzerhof, Phys. Rev. Lett. **77**, 3865 (1996).

[37] D. M. Ceperley and B. J. Alder, Phys. Rev. Lett. **45**, 566 (1980).

[38] J. P. Perdew and A. Zunger, Phys. Rev. B **23**, 5048 (1981).

[39] H. Jónsson, G. Mills, and K. W. Jacobsen, Nudged elastic band method for finding minimum energy paths of transitions, in *Classical and Quantum Dynamics in Condensed Phase Simulations*, edited by B. J. Berne, G. Ciccotti, and D. F. Coker (World Scientific, Singapore, 1998), Chap. 16, pp. 385–404.

[40] M. Methfessel and A. T. Paxton, Phys. Rev. B **40**, 3616 (1989).

[41] H. J. Monkhorst and J. D. Pack, Phys. Rev. B **13**, 5188 (1976).

[42] M. E. Tuckerman, B. J. Berne, G. J. Martyna, and M. L. Klein, J. Chem. Phys. **99**, 2796 (1993).

[43] M. E. Tuckerman, *Statistical Mechanics: Theory and Molecular Simulation* (Oxford University Press, Oxford, 2010), Chap. 12.

[44] D. Marx and M. Parrinello, J. Chem. Phys. **104**, 4077 (1996).

[45] M. Shiga, M. Tachikawa, and S. Miura, J. Chem. Phys. **115**, 9149 (2001).

[46] J. Cao and G. J. Martyna, J. Chem. Phys. **104**, 2028 (1996).

[47] S. Nosé, J. Chem. Phys. **81**, 511 (1984); W. G. Hoover, Phys. Rev. A **34**, 2499 (1986); D. J. Tobias, G. J. Martyna, and M. L. Klein, J. Phys. Chem. **97**, 12959 (1993).

[48] G. J. Martyna, M. E. Tuckerman, D. J. Tobias, and M. L. Klein, Mol. Phys. **87**, 1117 (1996).

[49] M. E. Tuckerman and D. Marx, Phys. Rev. Lett. **86**, 4946 (2001).

[50] M. Shiga and H. Fujisaki, J. Chem. Phys. **136**, 184103 (2012).

[51] C. Wert and C. Zener, Phys. Rev. **76**, 1169 (1949).

[52] E. Wimmer, W. Wolf, J. Sticht, P. Saxe, C. B. Geller, R. Najafabadi, and G. A. Young, Phys. Rev. B **77**, 134305 (2008).

[53] K. Klyukin, M. G. Shelyapina, and D. Fruchart, J. Alloys Compd. **644**, 371 (2015).

[54] D. R. Trinkle, Philos. Mag. **96**, 2714 (2016).

[55] See Supplemental Material at http://link.aps.org/supplemental/10.1103/PhysRevB.97.014102 for additional information on the free energy profiles for H migration in fcc Pd over a wide temperature range, which includes Refs. [23,56].

[56] D. Di Stefano, M. Mrovec, and C. Elsässer, Phys. Rev. B **92**, 224301 (2015).

[57] M. Shiga and W. Shinoda, J. Chem. Phys. **123**, 134502 (2005).

[58] C. P. Herrero and R. Ramírez, Phys. Rev. B **63**, 024103 (2000).

[59] B. G. A. Brito, L. Cândido, G.-Q. Hai, and F. M. Peeters, Phys. Rev. B **92**, 195416 (2015).

[60] C. P. Herrero and R. Ramírez, J. Chem. Phys. **148**, 102302 (2018).

[61] W. Drexel, A. Murani, and D. Tocchetti, J. Phys. Chem. Solids **37**, 1135 (1976); J. J. Rush, J. M. Rowe, and D. Richter, Z. Phys. B **55**, 283 (1984); J. M. Rowe, J. J. Rush, J. E. Schirber, and J. M. Mintz, Phys. Rev. Lett. **57**, 2955 (1986).

[62] H. Mehrer, *Diffusion in Solids: Fundamentals, Methods, Materials, Diffusion-Controlled Processes* (Springer, Berlin, 2007), Chap. 4, pp. 55–67.

[63] E. Pollak, J. Chem. Phys. **95**, 533 (1991).

[64] G. L. Powell and J. R. Kirkpatrick, Phys. Rev. B **43**, 6968 (1991).

[65] H. Hagi, Mem. Fukui Inst. Technol. **35**, 95 (2005).

[66] J. Völkl, G. Wollenweber, K.-H. Klatt, and G. Alefeld, Z. Naturforsch. A **26**, 922 (1971).

[67] H. Eyring, J. Chem. Phys. **3**, 107 (1935).

[68] G. Sicking, J. Less-Common Met. **101**, 169 (1984).